Computer Methods in Biomechanics and Biomedical Engineering, 2016
Vol. 19, No. 5, 465–473, http://dx.doi.org/10.1080/10255842.2015.1041022

The sensitivity of nonlinear computational models of trabecular bone to tissue level constitutive model

Andrew P. Baumann[1], Xiutao Shi[2], Ryan K. Roeder[3] and Glen L. Niebur*

Department of Aerospace and Mechanical Engineering, Bioengineering Graduate Program, University of Notre Dame, 147 Multidisciplinary Research Building, Notre Dame, IN 46556, USA

(*Received 20 July 2014; accepted 11 April 2015*)

Microarchitectural finite element models have become a key tool in the analysis of trabecular bone. Robust, accurate, and validated constitutive models would enhance confidence in predictive applications of these models and in their usefulness as accurate assays of tissue properties. Human trabecular bone specimens from the femoral neck ($n = 3$), greater trochanter ($n = 6$), and lumbar vertebra ($n = 1$) of eight different donors were scanned by μ-CT and converted to voxel-based finite element models. Unconfined uniaxial compression and shear loading were simulated for each of three different constitutive models: a principal strain-based model, Drucker–Lode, and Drucker–Prager. The latter was applied with both infinitesimal and finite kinematics. Apparent yield strains exhibited minimal dependence on the constitutive model, differing by at most 16.1%, with the kinematic formulation being influential in compression loading. At the tissue level, the quantities and locations of yielded tissue were insensitive to the constitutive model, with the exception of the Drucker–Lode model, suggesting that correlation of microdamage with computational models does not improve the ability to discriminate between constitutive laws. Taken together, it is unlikely that a tissue constitutive model can be fully validated from apparent-level experiments alone, as the calculations are too insensitive to identify differences in the outcomes. Rather, any asymmetric criterion with a valid yield surface will likely be suitable for most trabecular bone models.

Keywords: trabecular bone; constitutive model; finite element method; yield; nonlinear

Introduction

Computational modeling of trabecular bone is an important tool to augment mechanical testing via *in silico* or virtual experiments (van Rietbergen et al. 1998a, 1998b; Niebur et al. 2000; Niebur et al. 2002; Kosmopoulos and Keller 2003; Bayraktar et al. 2004b; Bayraktar and Keaveny 2004; Verhulp et al. 2008a; 2008b; Bevill and Keaveny 2009; Gong et al. 2011). The complex microscale morphology of trabecular bone has a dominant effect on the mechanics (Keaveny et al. 2001; Jaasma et al. 2002), necessitating models that capture geometric and material nonlinearities when simulating deformation beyond elastic limits. However, calibration and validation of these models is essential if they are to be used as predictive tools. Experimental methods can reveal trabecular bone's apparent-level properties (Townsend et al. 1975; Carter and Hayes 1976, 1977; Rice et al. 1988; Keaveny and Hayes 1993), but they cannot measure the associated tissue-level mechanics. Determining the location and severity of damage or plastic deformation within a trabeculae is experimentally infeasible. As such, directly validating nonlinear constitutive models remains difficult. Therefore, characterizing tissue-level yielding is beyond the scope of physical testing, and is presently best suited to numerical techniques.

The nonlinear response of trabecular bone has two underlying mechanisms: nonlinearly elastic behavior resulting from finite deformation of the porous structure (Townsend et al. 1975; Stölken and Kinney 2003; Bevill et al. 2006), and the nonlinear damaging and plastic deformation of the tissue. The effect of trabecular bending can be captured using finite kinematics formulations (Bevill et al. 2006), while the tissue-level damage-plasticity behavior has been simulated with several different constitutive models (Silva and Gibson 1997; Niebur et al. 2000; Bayraktar et al. 2004a; Hernandez et al. 2006; Mercer et al. 2006; Verhulp et al. 2008a; Wang et al. 2008; Kelly and McGarry 2012; Wolfram et al. 2012; Nawathe et al. 2013; Schwiedrzik et al. 2013). The key feature for capturing apparent-level behavior is the use of an asymmetric yield criterion (Pugh et al. 1973; Keaveny et al. 1994; Fenech and Keaveny 1999; Niebur et al. 2000), such as Mohr–Coulomb (Wang et al. 2008; Kelly and McGarry 2012), Drucker–Prager (Mercer et al. 2006; Kelly and McGarry 2012), or von Mises with pseudo-kinematic hardening term (Hernandez et al. 2006; Nawathe et al. 2013). While these models can be calibrated to capture the apparent-level mechanical behavior (Bayraktar et al. 2004b; Morgan et al. 2004;

*Corresponding author. Email: gniebur@nd.edu

Table 1. Human trabecular bone specimen properties. Mean (± SD) trabecular thickness (Tb.Th.), bone volume fraction (BV/TV), and structure model index (SMI).

	Tb.Th. (mm)	BV/TV	SMI
Femoral neck ($n = 3$)	0.23 (0.01)	0.19 (0.07)	1.38 (0.29)
Greater trochanter ($n = 6$)	0.21 (0.03)	0.18 (0.08)	1.52 (0.59)
Vertebra ($n = 1$)	0.19	0.14	1.88

Bevill et al. 2006; Kelly and McGarry 2012), confidence in the predictive ability of modeling requires that they also accurately capture the tissue-level mechanics. Moreover, accurate simulation of tissue mechanics could extend the application of models to predict damage locations (Nagaraja et al. 2005, 2007). The first step in identifying and calibrating constitutive models is to determine the sensitivity of the outcome variables to the boundary conditions and model parameters. Experiments can then be designed to highlight any differences, and thereby discriminate between the candidate theories. The objective of this study was to compare three potential constitutive models for trabecular tissue, and highlight differences in several outcome variables.

Materials and methods

Ten human trabecular bone specimens were modeled using a voxel-based finite element approach. The samples were taken from the femoral neck, greater trochanter, and lumbar vertebra of eight different donors, ensuring that a wide range of density and architecture were represented in the numerical models (Amling et al. 1996) (Table 1). Femur donors were male and female, aged 66–93, presenting no medical history of skeletal pathology or trauma, while the vertebra donor was anonymous. All tissue was obtained with donor's consent from the National Disease Research Interchange or from an anatomy lab (Indiana University).

The specimens were imaged by μ-CT (μCT-80, Scanco Medical AG, Brüttisellen, Switzerland) at 70 kVp, 114 μA and 400 ms integration time. Femur samples were imaged at 20 μm and the vertebra at 36 μm isotropic voxel size. Scans were smoothed by a Gaussian filter (support = 2, $\sigma = 1$) and segmented using a specimen-specific threshold corresponding to the bone volume fraction determined by Archimedes' principle (Morgan et al. 2004). The voxel size for the femoral samples was coarsened to 40 μm to reduce computation time. The mean trabecular thickness was greater than four times the voxel size for all models, as suggested for mesh convergence (Niebur et al. 1999; Tjong et al. 2012). Finite element models of cubic subregions, 5 mm × 5 mm × 5 mm, were generated by directly converting the bone voxels to 8-node hexahedral elements. The models had between 210,000 and 630,000 elements, and up to 2.6 million degrees of freedom. An isotropic elastic modulus of 15 GPa and a Poisson's ratio of 0.3 were assumed for the tissue.

The models were solved for two different boundary conditions. First, 1.2% unconfined uniaxial compression along the principal material direction, and then 1.5% shear strain in an axial–transverse plane direction (Figure 1). Three constitutive models were investigated. These included a principal strain-based damaging model (Niebur et al. 2000), Drucker–Lode, and Drucker–Prager (Figure 2(a)). The Drucker–Prager model was applied using both infinitesimal and finite kinematics such that each specimen was modeled four times for each loading mode.

The elastic-perfectly-damaging model with principal strain criterion was implemented in a custom parallelized code (Niebur et al. 2000; Niebur et al. 2002). Yielding occurred at an element integration point when the maximum or minimum principal strains exceeded specified limits. At these strain limits, the elastic modulus was isotropically reduced to achieve a tangent modulus equal to 5% of the initial value (Figure 2(b),(c)). Unloading followed the secant to the origin.

The Drucker–Lode model augments the von Mises criterion by incorporating the third invariant of deviatoric stress, resulting in a tension–compression asymmetry. The Drucker–Lode yield criterion is defined by,

$$\sqrt{2J_2} + \sqrt{\frac{27}{2}} b \frac{J_3}{J_2} = Y_0,$$

where J_2 and J_3 are the second and third invariants of deviatoric stress, respectively, and b and Y_0 are material constants. The strain hardening parameter was chosen to achieve a tangent modulus equal to 1% of the initial modulus in tension, which resulted in approximately 5% in

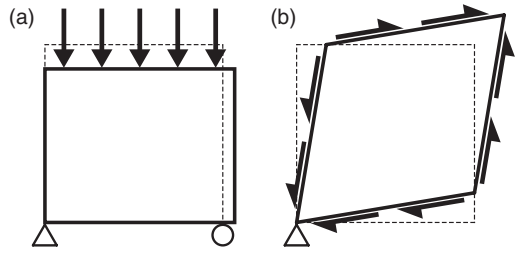

Figure 1. Schematic diagram showing boundary conditions applied to the finite element models to obtain (a) unconfined uniaxial compression and (b) shear in an axial–transverse plane.

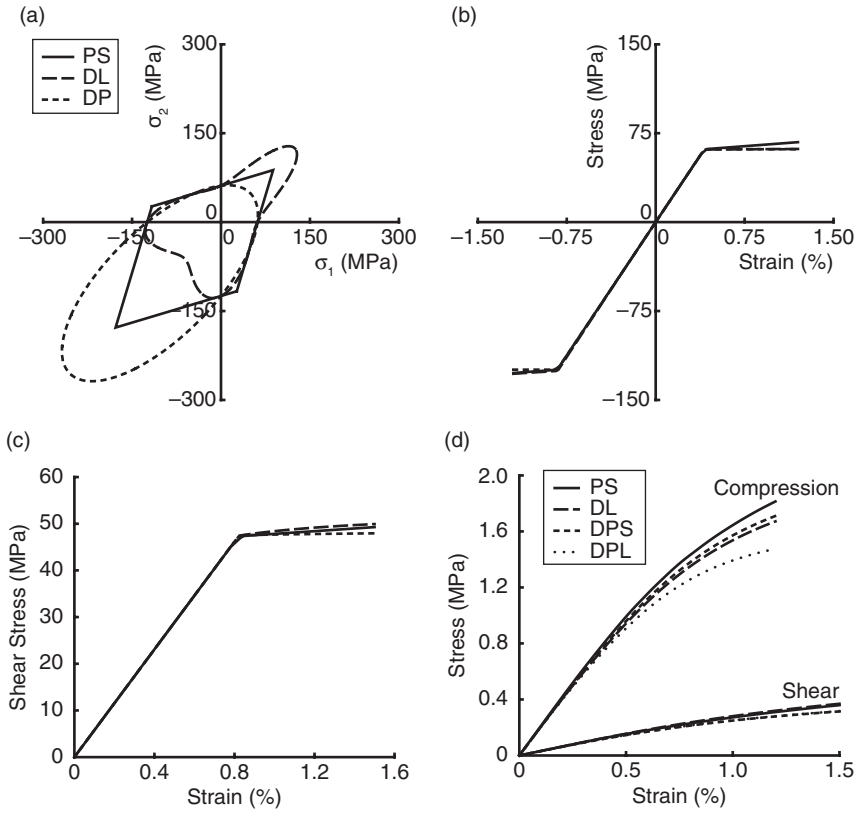

Figure 2. (a) Yield surfaces of the principal strain (PS), Drucker–Lode (DL), and Drucker–Prager (DP) constitutive models in principal stress space. Each criterion was calibrated to have the same yield strains in uniaxial tension and compression. Bilinear, asymmetric behavior of the yield criteria subject to (b) unconfined uniaxial compression and tension loading and (c) shear loading. The principal strain model had the tangent modulus equal to 5% of the original modulus at the yield point. The hardening modulus for the Drucker–Lode model was 1% of the original modulus. The Drucker–Prager model was perfectly plastic after yielding. (d) Representative stress–strain curves for a specimen from the greater trochanter with relatively low volume fraction (BV/TV = 0.12) to illustrate the differences between constitutive models at the apparent level.

compression. Models utilizing the Drucker–Lode yield criterion were solved using FEAP (Finite Element Analysis Program v8.1.a9, University of California, Berkeley).

The Drucker–Prager model similarly modifies the von Mises criterion to account for yielding asymmetry. The yield criterion is defined as,

$$\sqrt{2J_2} + \frac{1}{3}aI_1 = Y_0,$$

where J_2 is the second invariant of deviatoric stress, I_1 is the first invariant of total stress, and a and Y_0 are material constants. After exceeding the elastic limits, the model was perfectly plastic. Drucker–Prager models were solved with ADINA (ADINA R & D v8.8, Watertown, MA).

Yield properties for all models were chosen to achieve uniaxial tensile and compressive tissue yield strains of 0.41% and 0.83%, respectively (Bayraktar et al. 2004b). The results were compared at both the tissue and apparent levels. Apparent-level yield stress and strain were determined using the 0.2% offset method. At the tissue level, the quantity, mode (tension vs. compression), and location of yielded tissue were compared. All tissue-level comparisons were made at 1.2% and 1.5% strain in compression and shear, respectively, which are beyond the known yield strains. Intraspecimen comparisons of yielded tissue were quantified by the percentage of the total number of elements that yielded, and the congruence, defined as the percentage of yielded elements that were similarly yielded across two constitutive formulations. An exact match was considered when the elements were both subjected to tension ($I_1 > 0$) or to compression ($I_1 < 0$), while a relaxed criterion considered yielded tissue subjected to any stress state. In addition, the mean distance to the nearest element of equivalent yield state was calculated for non-congruent elements. Tissue was defined as yielded in the principal strain criterion if either the tensile or compressive strain limit was exceeded at any time. For the Drucker–Lode and Drucker–Prager models, yielded elements were identified by finding elements where the quantities $\sqrt{2J_2} +$

$\sqrt{(27/2)}b(J_3/J_2)$ or $\sqrt{2J_2} + (1/3)aI_1$ (in stress space) were greater than Y_0, respectively. Elements that had yielded and later unloaded were not counted.

Results were compared between constitutive formulations using repeated measures analysis of variance (ANOVA) (JMP 9.0.2, SAS Institute Inc., Cary, NC, USA). *Post hoc* comparisons between constitutive theories were performed using a paired *t*-test. The level of significance for all tests was set at $p < 0.05$.

Results

The mean calculated yield strains differed between the four formulations for both compressive and shear loading (Figure 3(a)). The apparent-level compressive yield strain calculated using the principal strain and Drucker–Prager small kinematics criteria were not statistically different ($p = 0.63$, ANOVA). Apparent-level shear yield strains were also not different between the large and small kinematics Drucker–Prager models ($p = 0.32$, ANOVA), while differences existed between the remaining models ($p < 0.0003$, ANOVA). Shear yield strains were larger than compressive yield strains ($p < 0.0001$, paired *t*-test), in agreement with experimental measurements (Fenech and Keaveny 1999; Ford and Keaveny 1996; Wu et al. 2013). Specimen yield strains were not correlated to volume fraction (BV/TV) ($p > 0.06$, ANOVA) (Figure 3 (b),(c)). For samples with BV/TV less than 0.2, the coefficient of variation of the apparent compressive yield strain was 0.15 compared to 0.06 for those with BV/TV greater than 0.2. However, there were not enough samples with low volume fraction to statistically validate this observation. Similarly, coefficient of variation of the apparent level shear yield strain was 0.11 for BV/TV less than 0.2 compared to 0.07 for BV/TV greater than 0.2.

The total amount of yielded tissue differed between models and loading modes (Figure 4). For compressive loading, the principal strain and Drucker–Prager model with finite kinematics were not different ($p = 0.15$, ANOVA). In contrast, models loaded in shear differed between all constitutive models ($p < 0.03$, ANOVA).

The locations of yielded tissue were sensitive to the yield criterion, but not to the kinematics formulation. Yielded elements had 41.7–88.7% agreement between formulations (Figure 5(a) and Table 2). Over 80% of the yielded elements were in agreement between the Drucker–Prager infinitesimal and finite kinematic formulations. In contrast, about 42% of yielded elements agreed between Drucker–Prager small and Drucker–Lode. Similar trends were observed in shear loading, with the greatest congruence achieved between Drucker–Prager small and Drucker–Prager large models and least congruence between Drucker–Lode and Drucker–Prager small models. Within compression models, the principal strain versus Drucker–Prager small and principal strain versus Drucker–Prager large model pairs were not different ($p = 0.13$, ANOVA), as were the principal strain versus Drucker–Prager large and Drucker–Lode versus principal strain model pairs ($p = 0.06$, ANOVA). All other congruence pairs in either compression or shear loading were significantly different ($p < 0.02$, ANOVA). The effects of BV/TV on congruence of yielded regions with respect to the Drucker–Prager large kinematics formu-

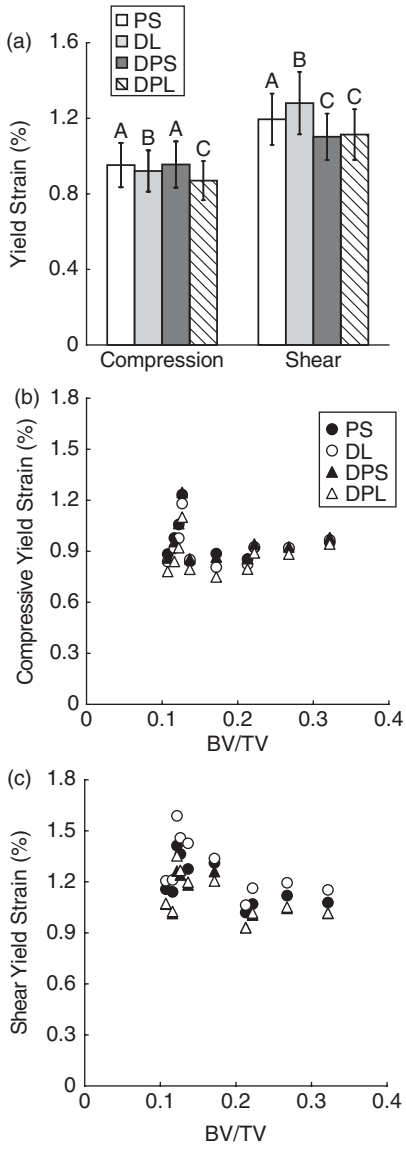

Figure 3. (a) Apparent-level yield strains (mean ± SD) for the four constitutive models (PS = principal strain, DL = Drucker–Lode, DPS = Drucker–Prager small, DPL = Drucker–Prager large). Differences between values not connected by the same letter were significantly different ($p < 0.05$, ANOVA). Apparent level (b) compression and (c) shear yield strains were not correlated to volume fraction (BV/TV), although the variation was greater for specimens with lower volume fractions (BV/TV < 0.2).

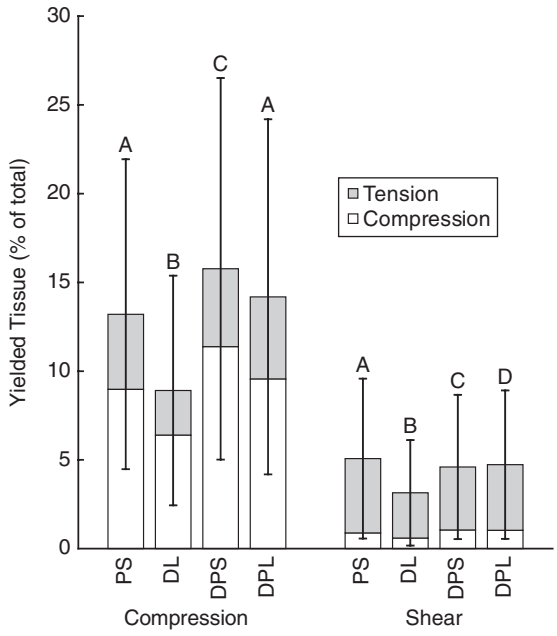

Figure 4. The total amount of tissue yielded (means of tension and compression yielding ± total SD) for each constitutive model (PS = principal strain, DL = Drucker–Lode, DPS = Drucker–Prager small, DPL = Drucker–Prager large) and loading mode at the end point of loading (1.2% and 1.5% strain in compression and shear, respectively). Bars not connected by the same letter were significantly different ($p < 0.05$, ANOVA).

lation revealed no correlations ($p > 0.06$, ANOVA) (Figure 5). Agreement between formulations was further evaluated by determining the distance from a yielded non-congruent element to the nearest element of equivalent yielding mode in the corresponding model (Figure 5(d)). The mean distance was approximately 2 elements (81.6 ± 35.3 μm) for compressive loading and slightly more (92.7 ± 53.6 μm) for shear ($p < 0.05$, paired t-test). The yielded regions in shear based on the Drucker–Lode criterion were farther from equivalent regions in other formulations.

Discussion

Nonlinear numerical analysis of trabecular bone relies on a suitable nonlinear constitutive model. Tissue yield properties with the proper incorporation of asymmetry can generally be calibrated to match apparent-level experimental results (Bayraktar et al. 2004b; Morgan et al. 2004; Bevill et al. 2006; Kelly and McGarry 2012). However, the sensitivity of outcome variables to these constitutive models is not known. The results of this study demonstrate that apparent-level experiments can delineate the tensile and compressive yield limits of the tissue constitutive model, but cannot entirely differentiate between constitutive models. Apparent-level yield properties of trabecular bone were dependent on the constitutive model. However, the large standard deviation in these measurements would make discerning one constitutive model from another unlikely, particularly in compressive loading. With the exception of the Drucker–Lode constitutive model, all criteria produced similar quantities of yielded tissue with nearly equivalent locations. Even if measuring the tissue-level yielding mode and location were experimentally feasible, one could only weakly separate the criteria based on these parameters. As such, fully validating a constitutive model at the tissue scale may be impractical. However, given the similarity of outcome variables, these results demonstrate it is reasonable to use any constitutive model that incorporates the underlying tissue strength asymmetry.

Tissue-level outcome variables of the Drucker–Lode constitutive model differed from the principal strain and Drucker–Prager models. When calibrated to the appropriate yield properties for bone, the Drucker–Lode criterion produced a concave yield surface, while the others were convex (Figure 2(a)). Concave yield surfaces are theoretically inadmissible because they permit evolution of unconnected elastic states, or continuous loading conditions that progress from yielded to unyielded states (Khan 1995). However, the three criteria still exhibited good agreement in the uniaxial tension, compression, and shear regions (within the second and fourth quadrants). This suggests that the majority of tissue yields in these modes, where the hydrostatic stress is low. The variation in the amount and location of yielded tissue must therefore be caused by the hydrostatic stress. It is here that the Drucker–Lode model is most different from the other criteria. The Drucker–Lode elastic region extended much further into the hydrostatic tension state, and was truncated in the hydrostatic compression state in comparison with the other criteria. As such, the lower fraction of yielded tissue in this model may have resulted from hydrostatic loading. Therefore, based on the tissue-scale outcome variables, it could be possible to differentiate the Drucker–Lode from the other constitutive models, given experimental methodologies that allow for tissue-scale determination of yielding mode and location.

The direct element-to-element comparison of yielded regions indicated that congruence is approximately 50% (Figure 5). This quantification, though, may be misleading. Yield maps of intraspecimen and intramode models revealed that the mode and general location of yielded tissue were similar for all constitutive models (Figure 6). The average distance to an equivalent yielded element between models was about 87 μm. Thus, while congruence may have only been about 50%, a region of similar yielding is within slightly more than two finite elements.

The results of this study complement previous studies investigating finite kinematics formulations (Stölken and Kinney 2003; Morgan et al. 2004; Bevill et al. 2006; Bevill

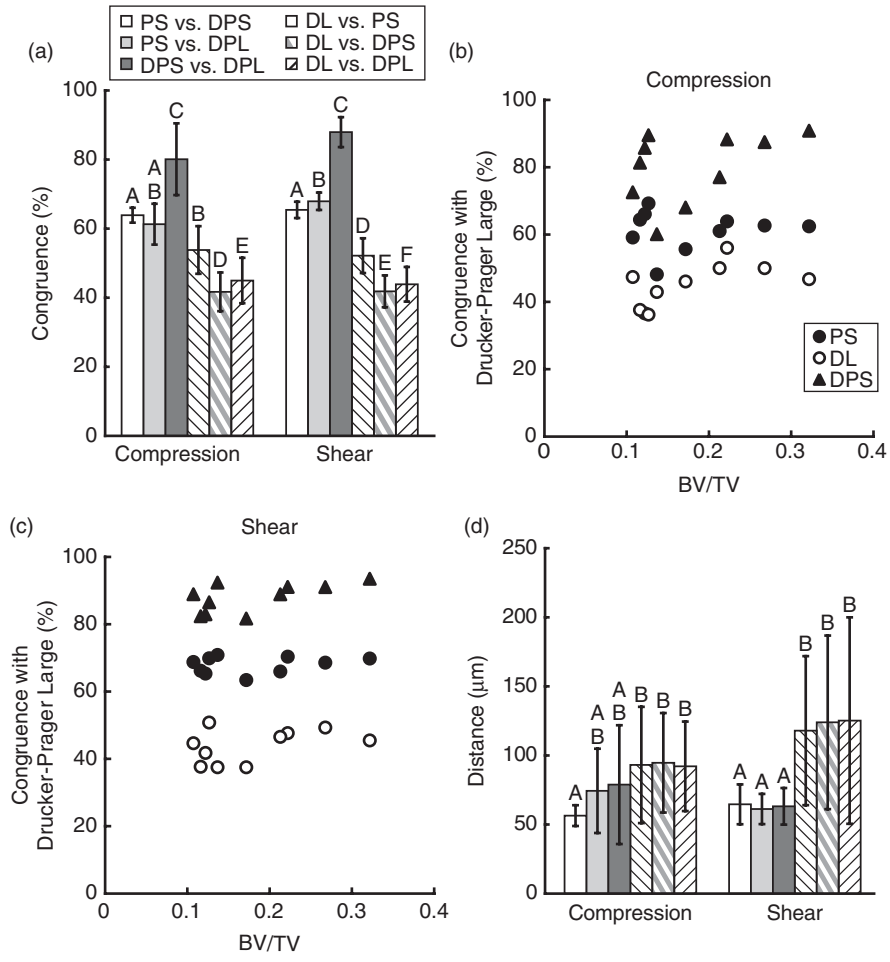

Figure 5. (a) Exact congruence (mean ± SD) of yielded elements between the four constitutive models (PS = principal strain, DL = Drucker–Lode, DPS = Drucker–Prager small, DPL = Drucker–Prager large). Specimen exact congruence with respect to the Drucker–Prager large constitutive model for (b) compression and (c) shear loading was not correlated to volume fraction (BV/TV). (d) Distance (mean ± SD) from a non-congruent yielded element to the nearest element of similar yielding mode in the corresponding model. Differences between values not connected by the same letter were statistically significant ($p < 0.05$, ANOVA).

Table 2. Mean (±SD) congruence percentage between constitutive models (PS = principal strain, DL = Drucker–Lode, DPS = Drucker–Prager small, DPL = Drucker–Prager large). Exact congruence requires that an element pair yield in the same mode (both in tension or both in compression). Relaxed congruence only requires that an element pair has yielded (both in tension, both in compression, or one in tension and the other in compression).

	Compression		Shear	
Congruence	Exact	Relaxed	Exact	Relaxed
PS vs. DL	53.8 (6.9)	55.0 (7.3)	52.2 (5.0)	53.7 (5.8)
PS vs. DPS	63.9 (2.2)	65.8 (1.8)	65.4 (2.4)	68.0 (2.5)
PS vs. DPL	61.3 (5.9)	63.4 (5.6)	67.9 (2.5)	70.3 (2.7)
DL vs. DPS	41.7 (5.6)	42.9 (6.0)	41.9 (4.6)	43.6 (5.3)
DL vs. DPL	45.0 (6.6)	46.3 (7.1)	43.9 (5.0)	45.6 (5.6)
DPS vs. DPL	80.1 (10.4)	81.5 (9.9)	88.0 (4.3)	88.7 (4.3)

et al. 2009; Nawathe et al. 2013). Finite kinematics were important for determining apparent level properties for low density samples in compression. However, the kinematic formulation did not influence the location of predicted tissue yielding. This further demonstrates the insensitivity of tissue-level outcomes to the model formulation in comparison to apparent-level outcomes. However, finite kinematics should be applied when models are used to complement physical experiments (Bevill et al. 2006, 2009; Bevill and Keaveny 2009).

The relative quantities of yielded tissue were similar to those found in previous studies. Much like the results of Sanyal et al. (2012) and Shi et al. (2009, 2010a, 2010b), our findings indicate that trabecular samples subjected to simulated compression exhibit a mixture of compressive and tensile yielding within the tissue, dominated by compressive yielding. This reflects the predominant

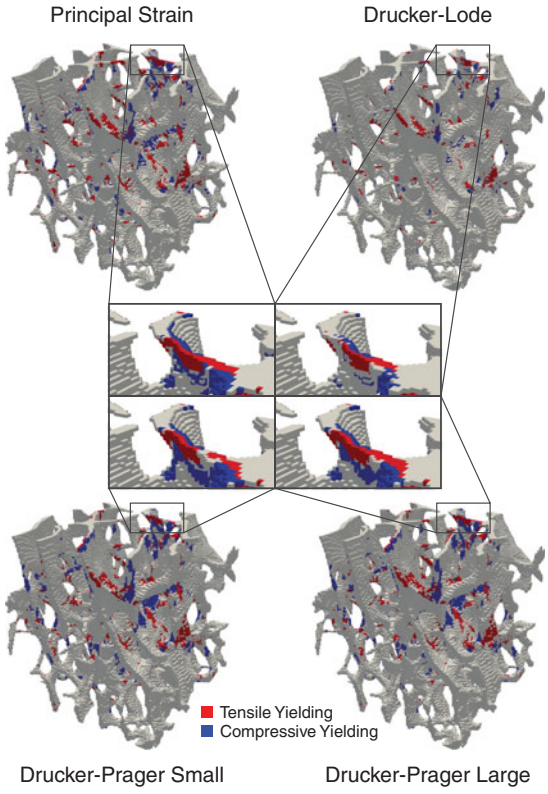

Figure 6. Yielded regions in a greater trochanter specimen as loaded in compression using the principal strain, Drucker–Lode, Drucker–Prager small strain, and Drucker–Prager large strain constitutive models. Insets depict the local differences in yielding on an element-by-element basis.

orientation of the trabecular tissue along the loading axis, such that bending of trabeculae is minimized (Niebur et al. 2000; Niebur et al. 2002; Bayraktar and Keaveny 2004; Bevill et al. 2009; Shi et al. 2009; 2010a, 2010b). In shear-loaded specimens, the majority of the tissue yielded in tension. This is consistent with predominant bending of trabeculae resulting in tensile yielding due to the asymmetry of the yield properties.

The femoral bone cores exhibited similar apparent-level compression yield strains to experimental results, while shear models underestimated the reported yield strains (Kopperdahl and Keaveny 1998; Bruyère Garnier et al. 1999; Morgan and Keaveny 2001; Bayraktar et al. 2004b; Rincón-Kohli and Zysset 2009; Wu et al. 2013). The apparent-level shear yield strains could be calibrated by adjusting the tensile yield strain in the criteria with little effect on apparent compressive yield properties. The compressive yield strain variability appeared qualitatively higher at lower volume fractions (Figure 3), but, unlike prior experimental studies, was uncorrelated to volume fraction (Bevill et al. 2009; Rincón-Kohli and Zysset 2009). However, this may be due to the lower sample size ($n = 10$). As such, differentiating between constitutive models based on apparent-level outcome variables may only be feasible at low volume fractions, if at all.

Additional loading modes could have revealed differences between the constitutive theories. Kelly and McGarry (2012) showed that for trabecular bone and analog loaded in uniaxial unconfined and confined compression, confining the specimen significantly influenced the non-linear response of trabecular bone. While Drucker–Prager and Mohr–Coulomb models were able to accurately predict the measured stress response for unconfined uniaxial compression, experimental and simulated confined compression showed that these models could not capture the measured response. If the specimens in this study had been loaded in confined compression, more elements may have been subjected to hydrostatic stresses which would be expected to highlight differences between constitutive models. Loading trabecular specimens perpendicular to the principal axis also influences the mode, quantity, and location of yielded trabecular tissue (Shi et al. 2009, 2010b). For example, compressing specimens in an off-axis mode induces greater quantities of tensile yielded tissue in transversely oriented trabeculae (Shi et al. 2009, 2010b). Simulated loading in this manner may have exposed more differences between the constitutive models.

The simulated yielding of trabecular specimens revealed that outcome variables are dependent upon the choice of nonlinear constitutive model. However, the differences between the constitutive models were relatively small. Tissue asymmetry dominated the apparent-level response, and tissue-level yielding was only able to discern criteria with major differences in the yield surface. Given that the yield criteria primarily differ in the locations of yielded tissue, methods to accurately measure yielding or damage volumetrically (Wang et al. 2007; Leng et al. 2008; Lambers et al. 2013) are needed to differentiate the models. Even with such tools, several criteria may give suitable results. Indeed, the criteria predict similar amounts, modes, and locations of yielded tissue when the yield surface is convex, and any such asymmetric criterion will perform reasonably well for most bone biomechanics applications.

Conflict of interest disclosure statement

The authors have nothing to disclose.

Funding

This work was partially supported by the National Institutes of Health [grant number AR052008]; and U.S. Army Telemedicine & Advanced Technology Research Center [grant number W81XWH-09-1-0741].

Notes

1. Email: abaumann@nd.edu

2. Email: xshi3@alumni.nd.edu
3. Email: rroeder@nd.edu

References

Amling M, Herden S, Pösl M, Hahn M, Ritzel H, Delling G. 1996. Heterogeneity of the skeleton: comparison of the trabecular microarchitecture of the spine, the iliac crest, the femur, and the calcaneus. J Bone Miner Res. 11(1):36–45. doi:10.1002/jbmr.5650110107.

Bayraktar HH, Gupta A, Kwon RY, Papadopoulos P, Keaveny TM. 2004a. The modified super-ellipsoid yield criterion for human trabecular bone. J Biomech Eng. 126(6):677–684. doi:10.1115/1.1763177.

Bayraktar HH, Keaveny TM. 2004. Mechanisms of uniformity of yield strains for trabecular bone. J Biomech. 37(11):1671–1678. doi:10.1016/j.jbiomech.2004.02.045.

Bayraktar HH, Morgan EF, Niebur GL, Morris GE, Wong EK, Keaveny TM. 2004b. Comparison of the elastic and yield properties of human femoral trabecular and cortical bone tissue. J Biomech. 37(1):27–35. doi:10.1016/S0021-9290(03)00257-4.

Bevill G, Eswaran SK, Gupta A, Papadopoulos P, Keaveny TM. 2006. Influence of bone volume fraction and architecture on computed large-deformation failure mechanisms in human trabecular bone. Bone. 39(6):1218–1225. doi:10.1016/j.bone.2006.06.016.

Bevill G, Farhamand F, Keaveny TM. 2009. Heterogeneity of yield strain in low-density versus high-density human trabecular bone. J Biomech. 42(13):2165–2170. doi:10.1016/j.jbiomech.2009.05.023.

Bevill G, Keaveny TM. 2009. Trabecular bone strength predictions using finite element analysis of micro-scale images at limited spatial resolution. Bone. 44(4):579–584. doi:10.1016/j.bone.2008.11.020.

Bruyère Garnier K, Dumas R, Rumelhart C, Arlot ME. 1999. Mechanical characterization in shear of human femoral cancellous bone: torsion and shear tests. Med Eng Phys. 21(9):641–649.

Carter DR, Hayes WC. 1976. Bone compressive strength: the influence of density and strain rate. Science. 194(4270):1174–1176. doi:10.1126/science.996549.

Carter DR, Hayes WC. 1977. The compressive behavior of bone as a two-phase porous structure. J Bone Joint Surg Am. 59(7):954–962.

Fenech CM, Keaveny TM. 1999. A cellular solid criterion for predicting the axial-shear failure properties of bovine trabecular bone. J Biomech Eng. 121(4):414–422. doi:10.1115/1.2798339.

Ford CM, Keaveny TM. 1996. The dependence of shear failure properties of trabecular bone on apparent density and trabecular orientation. J Biomech. 29(10):1309–1317. doi:10.1016/0021-9290(96)00062-0.

Gong H, Zhang M, Fan Y. 2011. Micro-finite element analysis of trabecular bone yield behavior – effects of tissue nonlinear material properties. J Mech Med Biol. 11(3):563–580. doi:10.1142/S0219519411004010.

Hernandez CJ, Gupta A, Keaveny TM. 2006. A biomechanical analysis of the effects of resorption cavities on cancellous bone strength. J Bone Miner Res. 21(8):1248–1255. doi:10.1359/jbmr.060514.

Jaasma MJ, Bayraktar HH, Niebur GL, Keaveny TM. 2002. Biomechanical effects of intraspecimen variations in tissue modulus for trabecular bone. J Biomech. 35(2):237–246. doi:10.1016/S0021-9290(01)00193-2.

Keaveny TM, Hayes WC. 1993. A 20-year perspective on the mechanical properties of trabecular bone. J Biomech Eng. 115(4B):534–542. doi:10.1115/1.2895536.

Keaveny TM, Morgan EF, Niebur GL, Yeh OC. 2001. Biomechanics of trabecular bone. Annu Rev Biomed Eng. 3(1):307–333. doi:10.1146/annurev.bioeng.3.1.307.

Keaveny TM, Wachtel EF, Ford CM, Hayes WC. 1994. Differences between the tensile and compressive strengths of bovine tibial trabecular bone depend on modulus. J Biomech. 27(9):1137–1146. doi:10.1016/0021-9290(94)90054-X.

Kelly N, McGarry JP. 2012. Experimental and numerical characterisation of the elasto-plastic properties of bovine trabecular bone and a trabecular bone analogue. J Mech Behav Biomed Mater. 9:184–197. doi:10.1016/j.jmbbm.2011.11.013.

Khan AS. 1995. Continuum theory of plasticity. New York (NY): John Wiley & Sons.

Kopperdahl DL, Keaveny TM. 1998. Yield strain behavior of trabecular bone. J Biomech. 31(7):601–608. doi:10.1016/S0021-9290(98)00057-8.

Kosmopoulos V, Keller TS. 2003. Finite element modeling of trabecular bone damage. Comput Methods Biomech Biomed Eng. 6(3):209–216. doi:10.1080/1025584031000149089.

Lambers FM, Bouman AR, Rimnac CM, Hernandez CJ. 2013. Microdamage caused by fatigue loading in human cancellous bone: relationship to reductions in bone biomechanical performance. PLoS ONE. 8(12):e83662. doi:10.1371/journal.pone.0083662.

Leng H, Wang X, Ross RD, Niebur GL, Roeder RK. 2008. Micro-computed tomography of fatigue microdamage in cortical bone using a barium sulfate contrast agent. J Mech Behav Biomed Mater. 1(1):68–75. doi:10.1016/j.jmbbm.2007.06.002.

Mercer C, He MY, Wang R, Evans AG. 2006. Mechanisms governing the inelastic deformation of cortical bone and application to trabecular bone. Acta Biomater. 2(1):59–68. doi:10.1016/j.actbio.2005.08.004.

Morgan EF, Bayraktar HH, Yeh OC, Majumdar S, Burghardt A, Keaveny TM. 2004. Contribution of inter-site variations in architecture to trabecular bone apparent yield strains. J Biomech. 37(9):1413–1420. doi:10.1016/j.jbiomech.2003.12.037.

Morgan EF, Keaveny TM. 2001. Dependence of yield strain of human trabecular bone on anatomic site. J Biomech. 34(5):569–577. doi:10.1016/S0021-9290(01)00011-2.

Nagaraja S, Couse TL, Guldberg RE. 2005. Trabecular bone microdamage and microstructural stresses under uniaxial compression. J Biomech. 38(4):707–716. doi:10.1016/j.jbiomech.2004.05.013.

Nagaraja S, Lin ASP, Guldberg RE. 2007. Age-related changes in trabecular bone microdamage initiation. Bone. 40(4):973–980. doi:10.1016/j.bone.2006.10.028.

Nawathe S, Juillard F, Keaveny TM. 2013. Theoretical bounds for the influence of tissue-level ductility on the apparent-level strength of human trabecular bone. J Biomech. 46(7):1293–1299. doi:10.1016/j.jbiomech.2013.02.011.

Niebur GL, Feldstein MJ, Keaveny TM. 2002. Biaxial failure behavior of bovine tibial trabecular bone. J Biomech Eng. 124(6):699–705. doi:10.1115/1.1517566.

Niebur GL, Feldstein MJ, Yuen JC, Chen TJ, Keaveny TM. 2000. High-resolution finite element models with tissue strength asymmetry accurately predict failure of trabecular bone. J Biomech. 33(12):1575–1583. doi:10.1016/S0021-9290(00)00149-4.

Niebur GL, Yuen JC, Hsia AC, Keaveny TM. 1999. Convergence behavior of high-resolution finite element models of trabecular bone. J Biomech Eng. 121(6):629–635. doi:10.1115/1.2800865.

Pugh JW, Rose RM, Radin EL. 1973. A structural model for the mechanical behavior of trabecular bone. J Biomech. 6(6):657–670. doi:10.1016/0021-9290(73)90022-5.

Rice JC, Cowin SC, Bowman JA. 1988. On the dependence of the elasticity and strength of cancellous bone on apparent density. J Biomech. 21(2):155–168. doi:10.1016/0021-9290(88)90008-5.

Rincón-Kohli L, Zysset P. 2009. Multi-axial mechanical properties of human trabecular bone. Biomech Model Mechanobiol. 8(3):195–208.

Sanyal A, Gupta A, Bayraktar HH, Kwon RY, Keaveny TM. 2012. Shear strength behavior of human trabecular bone. J Biomech. 45(15):2513–2519. doi:10.1016/j.jbiomech.2012.07.023.

Schwiedrzik JJ, Wolfram U, Zysset PK. 2013. A generalized anisotropic quadric yield criterion and its application to bone tissue at multiple length scales. Biomech Model Mechanobiol. 12(6):1155–1168. doi:10.1007/s10237-013-0472-5.

Shi X, Liu XS, Wang X, Guo XE, Niebur GL. 2010a. Effects of trabecular type and orientation on microdamage susceptibility in trabecular bone. Bone. 46(5):1260–1266. doi:10.1016/j.bone.2010.02.005.

Shi X, Liu XS, Wang X, Guo XE, Niebur GL. 2010b. Type and orientation of yielded trabeculae during overloading of trabecular bone along orthogonal directions. J Biomech. 43(13):2460–2466. doi:10.1016/j.jbiomech.2010.05.032.

Shi X, Wang X, Niebur G. 2009. Effects of loading orientation on the morphology of the predicted yielded regions in trabecular bone. Ann Biomed Eng. 37(2):354–362. doi:10.1007/s10439-008-9619-4.

Silva MJ, Gibson LJ. 1997. Modeling the mechanical behavior of vertebral trabecular bone: effects of age-related changes in microstructure. Bone. 21(2):191–199. doi:10.1016/S8756-3282(97)00100-2.

Stölken JS, Kinney JH. 2003. On the importance of geometric nonlinearity in finite-element simulations of trabecular bone failure. Bone. 33(4):494–504. doi:10.1016/S8756-3282(03)00214-X.

Tjong W, Kazakia GJ, Burghardt AJ, Majumdar S. 2012. The effect of voxel size on high-resolution peripheral computed tomography measurements of trabecular and cortical bone microstructure. Med Phys. 39(4):1893–1903. doi:10.1118/1.3689813.

Townsend PR, Rose RM, Radin EL. 1975. Buckling studies of single human trabeculae. J Biomech. 8(3–4):199–201. doi:10.1016/0021-9290(75)90025-1.

van Rietbergen B, Majumdar S, Pistoia W, Newitt DC, Kothari M, Laib A, Ruegsegger P. 1998a. Assessment of cancellous bone mechanical properties from micro-FE models based on micro-CT, pQCT and MR images. Technol Health Care. 6(5–6):413–420.

van Rietbergen B, Odgaard A, Kabel J, Huiskes R. 1998b. Relationships between bone morphology and bone elastic properties can be accurately quantified using high-resolution computer reconstructions. J Orthop Res. 16(1):23–28. doi:10.1002/jor.1100160105.

Verhulp E, van Rietbergen B, Müller R, Huiskes R. 2008a. Indirect determination of trabecular bone effective tissue failure properties using micro-finite element simulations. J Biomech. 41(7):1479–1485. doi:10.1016/j.jbiomech.2008.02.032.

Verhulp E, van Rietbergen B, Müller R, Huiskes R. 2008b. Micro-finite element simulation of trabecular-bone post-yield behaviour – effects of material model, element size and type. Comput Methods Biomech Biomed Eng. 11(4):389–395. doi:10.1080/10255840701848756.

Wang X, Allen MR, Burr DB, Lavernia EJ, Jeremić B, Fyhrie DP. 2008. Identification of material parameters based on Mohr–Coulomb failure criterion for bisphosphonate treated canine vertebral cancellous bone. Bone. 43(4):775–780. doi:10.1016/j.bone.2008.05.023.

Wang X, Masse DB, Leng H, Hess KP, Ross RD, Roeder RK, Niebur GL. 2007. Detection of trabecular bone microdamage by micro-computed tomography. J Biomech. 40(15):3397–3403. doi:10.1016/j.jbiomech.2007.05.009.

Wolfram U, Gross T, Pahr DH, Schwiedrzik J, Wilke HJ, Zysset PK. 2012. Fabric-based Tsai–Wu yield criteria for vertebral trabecular bone in stress and strain space. J Mech Behav Biomed Mater. 15:218–228. doi:10.1016/j.jmbbm.2012.07.005.

Wu Z, Laneve AJ, Niebur GL. 2013. In vivo microdamage is an indicator of susceptibility to initiation and propagation of microdamage in human femoral trabecular bone. Bone. 55(1):208–215. doi:10.1016/j.bone.2013.02.019.